molecular pharmaceutics

Communication

pubs.acs.org/molecularpharmaceutics

Shape-Controlled Paclitaxel Nanoparticles with Multiple Morphologies: Rod-Shaped, Worm-Like, Spherical, and Fingerprint-Like

Yongjun Wang,[*,‡,#] Dun Wang,[§,#] Qiang Fu,[‡] Dan Liu,[§] Yan Ma,[∥] Kelly Racette,[†] Zhonggui He,[‡] and Feng Liu[†,⊥]

[†]Division of Molecular Pharmaceutics, Eshelman School of Pharmacy, University of North Carolina at Chapel Hill, Pharmacy Lane, Chapel Hill, North Carolina27599, United States

[‡]School of Pharmacy, Shenyang Pharmaceutical University, 103 Wenhua Road, Shenyang 110016, China

[§]Key Laboratory of Structure-Based Drug Design and Discovery, Ministry of Education, Shenyang Pharmaceutical University, 103 Wenhua Road, Shenyang 110016, China

[∥]School of Chinese Materia Medica, Guangzhou University of Chinese Medicine, 232 Waihuan East Road, Guangzhou 510006, China

Supporting Information

ABSTRACT: Although many nanocarriers have been developed to encapsulate paclitaxel (PTX), the drug loading and circulation time *in vivo* always are not ideal because of its rigid "brickdust" molecular structure. People usually concentrate their attention on the spherical nanocarriers, here paclitaxel nanoparticles with different geometries were established through the chemical modification of PTX, nanoprecipitation, and core-matched cargos. Previously we have developed rod-shape paclitaxel nanocrystals using block copolymer, pluronic F127. Unfortunately, the pharmacokinetic (PK) profile of PTX nanocrystals is very poor. However, when PTX was replaced by its prodrug, the geometry of the nanoparticles changed from rod-shaped to worm-like. The worm-like nanoparticles can be further changed to spherical nanoparticles using the nanoprecipitation method, and changed to fingerprint-like nanoparticles upon the addition of the core-matched PTX. The nanoparticles with nonspherical morphologies, including worm-like nanoparticles and fingerprint-like nanoparticles, offer significant advantages in regards to key PK parameters *in vivo*. More important, in this report the application of the core-matching technology in creating a core-matched environment capable of controlling the *in vivo* PK of paclitaxel was demonstrated, and it revealed a novel technique platform to construct nanoparticles and improve the poor PK profiles of the drugs.

KEYWORDS: *geometry, paclitaxel, worm-like, fingerprint-like, pharmacokinetics, circulation*

Traditional drug delivery systems mainly focus on spherical carriers that are between 10 and 200 nm in diameter, the dependence of accumulation in the tumor on the "enhanced permeability and retention" (EPR) effect results in the emphasis on the size of the particles. The impact of the geometry of the carriers on their *in vivo* behavior is intriguing and warrants further study, in particular, the effect of geometry on circulation time,[1,2] the interaction of particles with target cells,[3,4] cellular uptake of the particles, and subcellular trafficking of the cargo.[5,6] In addition to spherical carriers, developed geometries include, but are not limited to, flat disks, rods or cylinders, and worm-like micelles (filomentous micelles).[7−10] Amphiphilic block copolymers have diversified structures that are precisely designed and are typically used to construct nonspherical carriers. It is well-known that the size and shape of polymeric nanoparticles (NPs) can be designed through the control of the balance of hydrophilic/hydrophobic components of the polymer. However, here, for the first time, we show that the morphology can be transformed through changing the encapsulated cargo or offering a matching environment to encapsulate the cargo. Subsequently, the circulation time of the encapsulated drugs is significantly prolonged.

Paclitaxel (PTX) is an anticancer agent used to clinically treat a variety of solid tumors. However, two major defects make the application of PTX in cancer therapy difficult. The first is the extremely low water solubility of PTX, which is less than 1 μg/mL. The other is the inferior pharmacokinetics (PK) of PTX *in vivo*. At this time, only two PTX-based drugs have been approved by the FDA for use in the treatment of cancer. Unfortunately, both therapies have very poor PK, more than 95% of PTX is cleared from the blood within 10 min of injection. So far, various approaches have been developed, including liposomes, emulsions, polymer NPs, lipid NPs, conjugates, etc.[11−16] However, the improvement of PK of PTX is always a challenge. In this study, we report the formation of nonspherical structures from a mixture of amphiphilic block copolymers, pluronic F127, and PTX prodrug and/or PTX. These nonspherical structures exhibit PK profiles that are significantly improved over traditionally shaped particles *in vivo*.

Received: June 19, 2014
Revised: August 30, 2014
Accepted: September 4, 2014
Published: September 4, 2014

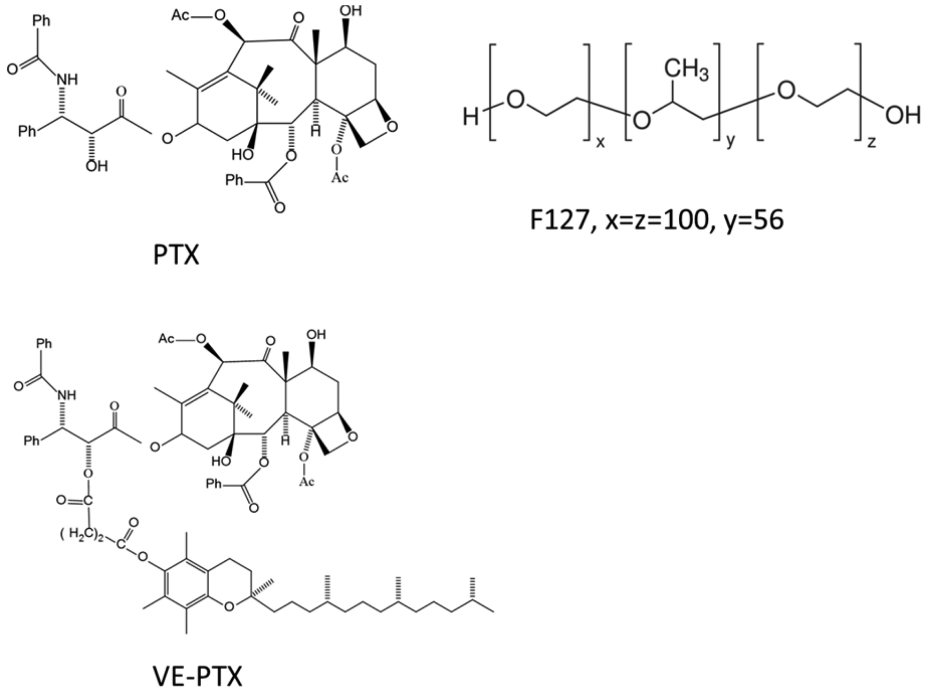

Figure 1. Chemical structures of PTX, VE-PTX, and F127.

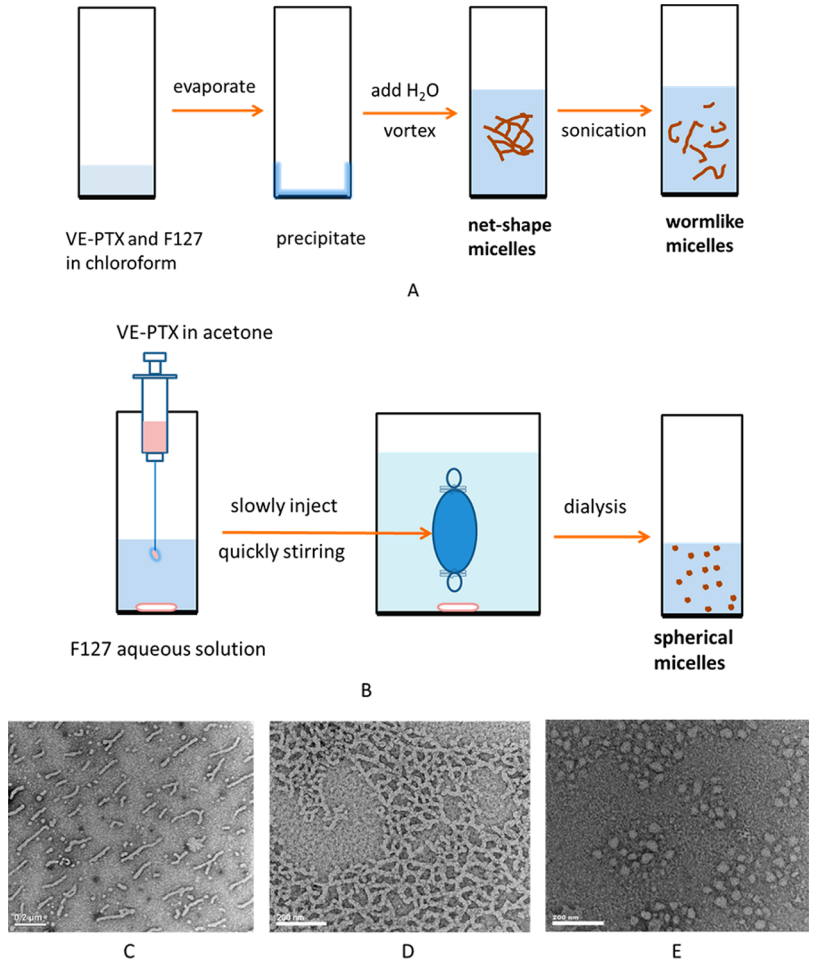

Figure 2. Schematic illustration of preparation procedure for the worm-like NPs (A) and the VE-PTX spherical NPs (B). TEM images of worm-like NPs (C), the net-shaped NPs (D), and spherical NPs (E). Scale bar for TEM images (C,D,E) is 200 nm.

dx.doi.org/10.1021/mp500436p | *Mol. Pharmaceutics* 2014, 11, 3766−3771

PTX molecules consist of a rigid taxane ring and a flexible side chain (Figure 1), qualities that make them insoluble in both water and oil.[17] Encapsulation of PTX into nanocarriers with high loading efficiency is difficult because of its physicochemical properties. Our group has developed rod-shaped PTX nanocrystals (Figure S1, Supporting Infomation) with a diameter of ~100 nm using block copolymer, pluronic F127, which have a very high efficiency of drug loading, the ability to overcome multiple drug resistance (MDR), and are easily producible.[18,19] Unfortunately, PTX nanocrystals had a PK profile even worse than that of Taxol and Abraxane. In our lab, in order to promote its oil solubility, vitamin E (VE) was conjugated to PTX (VE-PTX, Figure 1), and a core-matched VE-PTX nanoemulsion with long circulation *in vivo* was developed, and significant *in vivo* antitumor efficacy was achieved.[20,21] With the desire to take advantage of PTX nanocrystals, we replaced PTX with VE-PTX. Interestingly, the morphology changed from rod-shape to worm-like.

Figure 2A illustrates the synthetic process for producing VE-PTX worm-like NPs that is the same as the process for producing PTX nanocrystals. Images obtained from transmission electron microscopy (TEM) show that the F127/VE-PTX mixture forms particles with a worm-like assembled structure (Figure 2C). In the process of preparing the worm-like NPs, we can also observe the formation of net-shaped intermediate nanostructures (Figure 2D). The morphology of formulated nanostructures can be manipulated through making changes to either the structural characteristics of the copolymers or the methods used to prepare the nanostructures.[22,23] Here we focus on the latter, successfully changing the geometry of NPs from worm-like to spherical through the use of a different method of preparation (nanoprecipitation method). As illustrated in Figure 2B, VE-PTX acetone solution was slowly injected into the rapidly stirring F127 aqueous; then in order to remove the acetone, the solution was placed in dialysis bag (MWCO = 3500), which was immersed in water. The external medium was changed periodically over the next 48 h. TEM images confirmed that the nanoprecipitation method created NPs with a spherical morphology (Figure 2E).

The similarities between the components of the spherical and worm-like NPs may provide unique insight into the role of the shape of nanocarriers in their *in vivo* PK. Worm-like NPs appeared to circulate longer in the blood (Figure 3). The PK parameters for VE-PTX data were calculated and presented in Table 1. The difference between the $AUC_{0-\infty}$ values of VE-PTX in worm-like and spherical NPs was 6.5-fold. The worm-like NPs increased the $t_{1/2}$ of VE-PTX to 12.11 h relative to spherical NPs (4.74hours). In order to enhance the circulation of nanocarriers in the blood, a surfactant, DSPE-PEG2000, is typically used to coat the carrier such as liposomes, polymer NPs, lipid NPs, and emulsions. In our previous study, a VE-PTX nanoemulsion coated with DSPE-PEG2000 also exhibited a significantly improved PK profile.[20] However, as shown in Figure 3 and Table 1, the nanoemulsion that prolonged the PK profile of VE-PTX may compare to that of the drugs carried by spherical NPs, but still did not compare to that of the worm-like NPs. The reason for these results is thought to be the flexibility and elongation of the worm-like NPs, which enables them to align with the blood flow and avoid vascular collisions and filtration, and are internalized less readily by macrophages.[2]

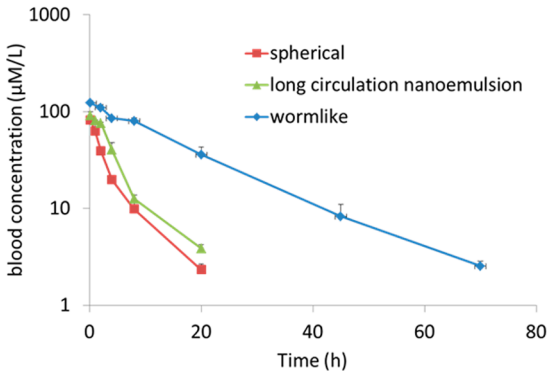

Figure 3. Blood concentration−time curves of VE-PTX in mice after IV administration of various VE-PTX formulaitons at a dose of 11.7 μM/kg (n = 3).

On the basis of the compatibility of the nanocarriers' cores, their cargo, and the PEGylated molecules, we developed the core-matched technology (CMT).[20,21] We have developed these core-matched nanocarriers of therapeutic and imaging modalities through the conjugation of all of the components (functional molecules and PEG) to a molecule representative of the core of the nanocarriers. This technique has been successfully applied to various types of nanocarriers to improve drug loading and circulation in the blood compared to traditional PEGylated nanocarriers. In the application of the CMT, we assume that, if a PTX matching environment is provided, PTX will be retained in the carrier and the prolonged circulation of PTX *in vivo* will be achieved.

Theoretically, the PTX portion of VE-PTX in worm-like NPs could provide a matching environment for free PTX. As PTX was added into the worm-like NPs (synthetic process was shown in Figure S2, Supporting Information), their morphology changed into fingerprint-like structures (F127/VE-PTX/PTX = 1:3:1, molar ratio) (Figure 4A). The TEM images and our conceptual drawing (Figure 4B) illustrate that the fingerprint-like NPs are multilamellar vesicles. It is interesting that the worm-like NPs change into fingerprint-like NPs, which include multiple water phases. We presume that the increased rigidity or hydrophobicity in response to adding PTX to the worm-like NPs imparts enough curvature to the NPs, which leads to the formation of the fingerprint-like morphology.[24,25] In order to demonstrate that there are water phases in the fingerprint-like NPs, we prepared two solutions. The first was a mixture of the fingerprint-like NPs solution with a water-soluble sulforhodamine B (SRB) solution (solution I). The second was created during the preparation of the fingerprint-like NPs, the precipitate was hydrated using a SRB solution (solution II). Both solutions were respectively passed through a 5 cm Sephadex G-50 column. Approximately 10 mL of PBS buffer was added in a dropwise fashion to the top of the column, and the eluate solution was collected (eluates I and II correspond to solutions I and II, respectively). SRB that was not encapsulated in the particles was separated from the fingerprint-like NPs through size-exclusion chromatography.

The fluorescence intensity of collected fractions was determined using a fluorescence spectrophotometer (Figure 4C). The first peak, at 1 mL, corresponds to the eluted fingerprint-like NPs, and the second peak, at 5 mL, corresponds to the SRB that was not encapsulated. However, the small peak of eluate II (green line) disappears after determining its fluorescence. The fluorescence of SRB in the fingerprint NPs (eluate II) was not detected; the reason was that fluorescence would self-quenched at high concentrations due to dye−dye

Table 1. PK Parameters of PTX or VE-PTX in Mice at Various Drug Formulations[a]

formulation/drug	$AUC_{0-\infty}$	$AUMC_{0-\infty}$	MRT	$t_{1/2}$	T_{max}	Cl	V_D	C_{max}
worm-like/VE-PTX	2175.84 ± 316.67	34563.93 ± 8647.34	15.76 ± 1.68	12.11 ± 1.58	0.17	0.01 ± 0.00	0.09 ± 0.01	122.33 ± 7.60
spherical/VE-PTX	333.42 ± 42.57	1762.68 ± 357.91	5.26 ± 0.40	4.74 ± 0.83	0.17	0.04 ± 0.01	0.24 ± 0.01	81.82 ± 1.89
nanoemulsion /VE-PTX	499.72 ± 45.36	2419.04 ± 658.23	4.80 ± 0.88	3.44 ± 1.29	0.17	0.02 ± 0.01	0.11 ± 0.03	91.56 ± 8.62
fingerprint/PTX	213.05 ± 3.79	1513.71 ± 128.44	7.11 ± 0.73	6.08 ± 0.49	0.17	0.05 ± 0.01	0.48 ± 0.05	40.29 ± 1.61
Taxol/PTX	8.06 ± 2.37	10.55 ± 3.70	1.30 ± 0.08	0.94 ± 0.09	0.17	1.52 ± 0.45	2.02 ± 0.40	5.05 ± 1.07
nanocrystal/PTX	4.10 ± 0.41	6.30 ± 0.87	1.53 ± 0.06	1.16 ± 0.01	0.17	2.87 ± 0.28	4.81 ± 0.51	2.74 ± 0.16

[a]Parameters and units: area under the curve ($AUC_{0-\infty}$, μM/L h); area under the moment curve ($AUMC_{0-\infty}$, μM/L h^2); mean residence time ($MRT_{0-\infty}$, h); half-life ($t_{1/2}$, h); time of maximal concentration (T_{max}, h); total body clearance (Cl, L/h/kg); volume of distribution (V_D, L/kg) ; maximal concentration (C_{max}, μM/L)

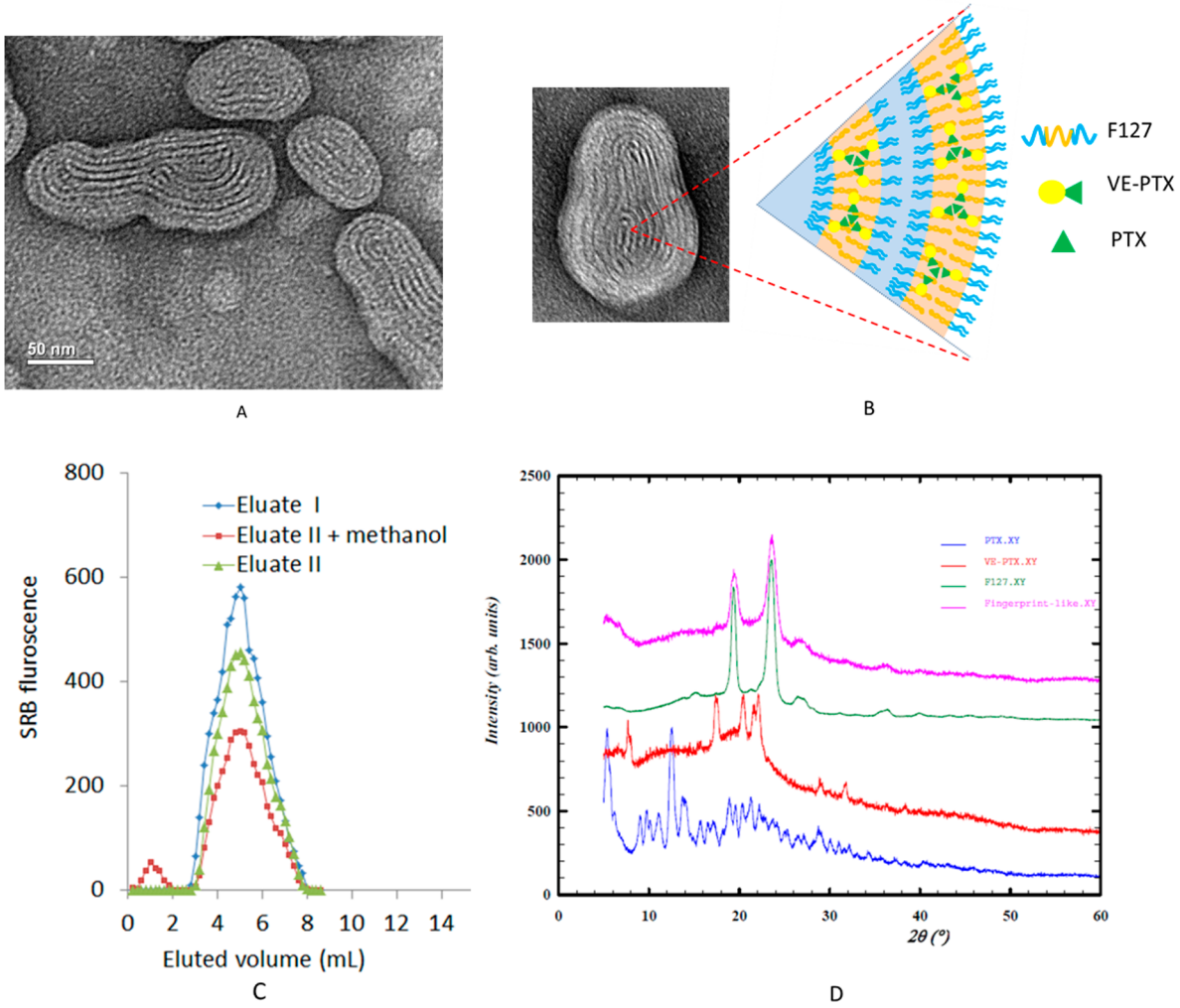

Figure 4. TEM images of the fingerprint-like NPs (A), and its speculated structural schematic representation (B). (C) Elution profiles on Sephadex G50 of solution I and solution II detected by fluorescence. PBS buffer was used as the eluent. The eluate was collected and separated into 0.2 mL samples per tube, followed by fluorescence measurement using a RF-551 spectrofluorometric detector (Shimadzu, Kyoto, Japan). (D) Powder XRD patterns of pure PTX, VE-PTX, F127, and fingerprint-like NPs.

interactions.[26,27] After eluate II was diluted with methanol (red line, the NPs was dissolved), the fluorescence was recovered. The results demonstrate that small amounts of the SRB solution were encapsulated in the water phase of the fingerprint-like NPs.

Powder X-ray diffraction (XRD) was performed to further study the physical state of PTX in the fingerprint-like NPs. As shown in Figure 4D, the Bragg peaks of PTX and VE-PTX within the fingerprint-like NPs disappear from the diffraction patterns, indicating the crystalline structure, which is evidence of the absence of crystalline PTX. The results indicated that PTX could be encapsulated in the fingerprint-like NPs that have an amorphous state.

The release profiles of PTX from fingerprint-like NPs *in vitro* were also assessed and compared to those of Taxol and PTX nanocrystals (Figure 5A). The release of PTX from fingerprint-like NPs and Taxol is more rapid than that of PTX nanocrystals, with pH 6.8 PBS buffer containing 0.05%

dx.doi.org/10.1021/mp500436p | *Mol. Pharmaceutics* 2014, 11, 3766−3771

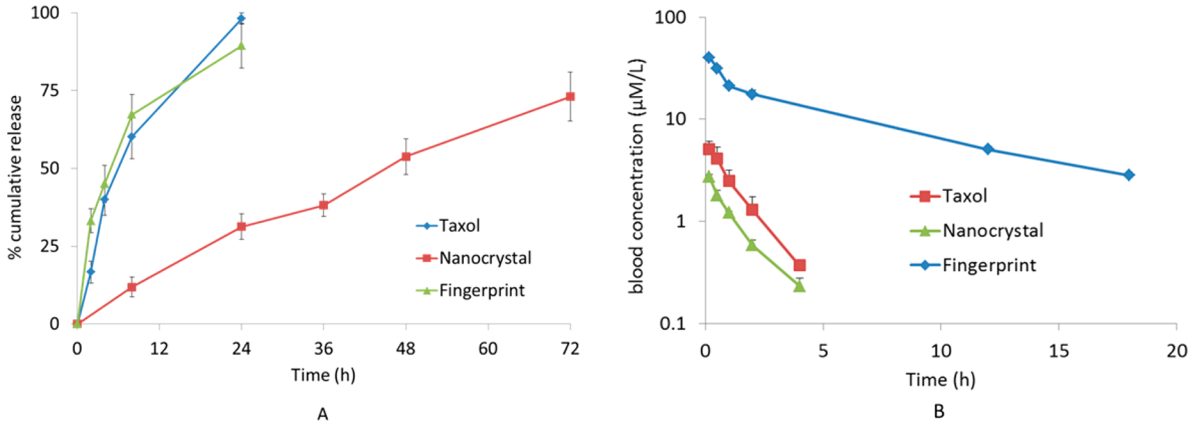

Figure 5. *In vitro* release profiles (A) and *in vivo* PK profiles (B) of PTX-loaded formulations. (A) Release profiles were determined using a dialysis method: dialysis membrane with a cutoff of a molecular weight between 12,000 and 14,000; release medium, 400 mL of pH 6.8 PBS buffer containing 0.05% Tween 80; paddle rotate speed, 100 rpm. (B) Blood concentration−time curves of PTX in mice after IV administration of various PTX formulaitons at a dose of 11.7 μM/kg (n = 3).

Tween 80 as dissolution media. The cumulative release of PTX from PTX nanocrystals after 8 h was only 11.9%, while the cumulative release from fingerprint-like NPs and Taxol was 67.3% and 60.2%, respectively. In Taxol, PTX was encapsulated in NPs of cremophor EL (the weight ratio of PTX to cremophor EL is 1:90), resulting in a rapid release. In fingerprint-like NPs, the amorphous state of PTX was assumed to improve the *in vitro* release.

Despite the rapid release of PTX *in vivo*, the fingerprint-like NPs circulate longer within the bloodstream than NPs of other structures (Figure 5B). For PTX nanocrystals, F127 absorbed to the surface of PTX nanocrystals may dissociate from the surface when the nanocrystals enter the bloodstream, resulting in rapid recognition of opsonin proteins and rapid elimination via phagocytic cells. Improved PK of PTX from the fingerprint-like NPs was attributed to the unique nanostructure. Rijcken and Letchford et al. demonstrated that PTX would be rapidly cleared from the blood within minutes, despite the encapsulation of PTX in NPs with increased hydrophobic block length of the copolymer or one type of micelle with a cross-linked core.[28] Although the carriers themselves were able to achieve prolonged circulation, PTX was rapidly partitioned out of the cores of the copolymer NPs or micelles with cross-linked cores. In contrast, the worm-like NPs provide a core-matched environment for PTX and enable the prolonged cirulation of PTX after the particles enter into circulation. The PK parameters were also shown in Table 1. Collectively, the fingerprint-like NPs increase the AUC, MRT, and $t_{1/2}$ and decrease the Cl and V_D of PTX. The fingerprint-like NPs significantly increased the AUC values of PTX, which were 26- and 52-fold of those AUC of Taxol and PTX nanocrystals, respectively. Long circulation would facilitate accumulation of the particles in the tumor and improve their therapeutic effect.

However, as the ratio of F127 to VE-PTX was fixed, and increasing the amount of PTX included, the PK of PTX gradually became poor (Figure S3, Supporting Information). Clearly, the increase of the amount of PTX affects the hydrophobic core of the fingerprint-like NPs and destabilizes its structure, decreasing the PK with the growth of the PTX nanocrystals (Figure S4, Supporting Information). The VE portion of VE-PTX in worm-like NPs also provides a matching environment for free VE, but as VE was added into the worm-like NPs, their morphology changed into heterogeneous, spherical particles instead of the fingerprint like NPs (Figure S5, Supporting Information).

In this study, we demonstrated that changes in morphology depend on the structure of the encapsulated compounds. More importantly, particles with nonspherical morphologies, including worm-like NPs and fingerprint-like NPs, offer significant advantages in regards to key PK parameters (AUC, MRT, and $t_{1/2}$). In fact, the AUC value of worm-like NPs achieved a 270- and 540-fold increase compared to Taxol and PTX nanocrystals (Table 1). Furthermore, on the basis of our CMT, the worm-like NPs provide a matching environment that encapsulates PTX molecules into the NPs. The application of the CMT in creating a core-matched environment capable of controlling the *in vivo* PK of parent drugs revealed a novel technique platform to improve the poor PK profiles of the drugs.

■ ASSOCIATED CONTENT

Ⓢ Supporting Information

Experimental details including preparation of various formulations, TEM images, *in vitro* release study, size exclusion chromatography of fingerprint-like NPs, power XRD, *in vivo* PK study, and supporting figures. This material is available free of charge via the Internet at http://pubs.acs.org.

■ AUTHOR INFORMATION

Corresponding Author

*(Y.W.) E-mail: wangyjspu@163.com.

Author Contributions

#Y.W. and D.W. contributed equally to this work.

Notes

The authors declare no competing financial interest.

⊥Deceased. Dedicated to the memory of Professor Feng Liu, Ph.D., 1955−2014.

■ ACKNOWLEDGMENTS

This work was supported by the National Cancer Institute−National Institutes of Health (5R01CA149387).

■ REFERENCES

(1) Christian, D. A.; Cai, S.; Garbuzenko, O. B.; Harada, T.; Zajac, A. L.; Minko, T.; Discher, D. E. Flexible Filaments for in Vivo Imaging and Delivery: Persistent Circulation of Filomicelles Opens the Dosage

Window for Sustained Tumor Shrinkage. *Mol. Pharmaceutics* **2009**, *6* (5), 1343−1352.
(2) Simone, E. A.; Dziubla, T. D.; Muzykantov, V. R. Polymeric Carriers: Role of Geometry in Drug Delivery. *Expert Opin. Drug Delivery* **2008**, *5* (12), 1283−1300.
(3) Loverde, S. M.; Klein, M. L.; Discher, D. E. Nanoparticle Shape Improves Delivery: Rational Coarse Grain Molecular Dynamics (rCG-MD) of Taxol in Worm-Like PEG-PCL Micelles. *Adv. Mater.* **2011**, n/a−n/a.
(4) Dalhaimer, P.; Engler, A. J.; Parthasarathy, R.; Discher, D. E. Targeted Worm Micelles. *Biomacromolecules* **2004**, *5* (5), 1714−1719.
(5) Geng, Y.; Dalhaimer, P.; Cai, S.; Tsai, R.; Tewari, M.; Minko, T.; Discher, D. E. Shape Effects of Filaments versus Spherical Particles in Flow and Drug delivery. *Nat. Nanotechnol.* **2007**, *2* (4), 249−55.
(6) Zhao, P.; Liu, L.; Feng, X.; Wang, C.; Shuai, X.; Chen, Y. Molecular Nanoworm with PCL Core and PEO Shell as a Non-spherical Carrier for Drug Delivery. *Macromol. Rapid Commun.* **2012**, *33* (16), 1351−1355.
(7) Zhang, W.; Sun, J.; Liu, Y.; Tao, M.; Ai, X.; Su, X.; Cai, C.; Tang, Y.; Feng, Z.; Yan, X.; Chen, G.; He, Z. PEG-Stabilized Bilayer Nanodisks As Carriers for Doxorubicin Delivery. *Mol. Pharmaceutics* **2014**, DOI: 10.1021/mp400566a.
(8) Bae, J.; Lawrence, J.; Miesch, C.; Ribbe, A.; Li, W.; Emrick, T.; Zhu, J.; Hayward, R. C. Multifunctional Nanoparticle-Loaded Spherical and Wormlike Micelles Formed by Interfacial Instabilities. *Adv. Mater.* **2012**, *24* (20), 2735−2741.
(9) Cardiel, J. J.; Dohnalkova, A. C.; Dubash, N.; Zhao, Y.; Cheung, P.; Shen, A. Q. Microstructure and Rheology of a Flow-Induced Structured Phase in Wormlike Micellar Solutions. *Proc. Natl. Acad. Sci. U.S.A.* **2013**, *110*, E1653−E1660.
(10) Toft, D. J.; Moyer, T. J.; Standley, S. M.; Ruff, Y.; Ugolkov, A.; Stupp, S. I.; Cryns, V. L. Coassembled Cytotoxic and Pegylated Peptide Amphiphiles Form Filamentous Nanostructures with Potent Antitumor Activity in Models of Breast Cancer. *ACS Nano* **2012**, *6*, 7956−7965.
(11) Lu, J.; Huang, Y.; Zhao, W.; Chen, Y.; Li, J.; Gao, X.; Venkataramanan, R.; Li, S. Design and Characterization of PEG-Derivatized Vitamin E as a Nanomicellar Formulation for Delivery of Paclitaxel. *Mol. Pharmaceutics* **2013**, *10* (8), 2880−2890.
(12) Lin, L. Y.; Karwa, A.; Kostelc, J. G.; Lee, N. S.; Dorshow, R. B.; Wooley, K. L. Paclitaxel-Loaded SCK Nanoparticles: An Investigation of Loading Capacity and Cell Killing Abilities in Vitro. *Mol. Pharmaceutics* **2012**, *9* (8), 2248−2255.
(13) Ganta, S.; Amiji, M. Coadministration of Paclitaxel and Curcumin in Nanoemulsion Formulations To Overcome Multidrug Resistance in Tumor Cells. *Mol. Pharmaceutics* **2009**, *6* (3), 928−939.
(14) Yuk, S. H.; Oh, K. S.; Cho, S. H.; Kim, S. Y.; Oh, S.; Lee, J. H.; Kim, K.; Kwon, I. C. Enhancement of the Targeting Capabilities of the Paclitaxel-Loaded Pluronic Nanoparticles with a Glycol Chitosan/Heparin Composite. *Mol. Pharmacol.* **2011**, *9* (2), 230−236.
(15) Luo, C.; Wang, Y.; Chen, Q.; Han, X.; Liu, X.; Sun, J.; He, Z. Advances of Paclitaxel Formulations Based on Nanosystem Delivery Technology. *Mini Rev. Med. Chem.* **2012**, *12* (5), 434−44.
(16) Koudelka, S.; Turanek, J. Liposomal Paclitaxel Formulations. *J. Controlled Release* **2012**, *163* (3), 322−34.
(17) Feng, S.-S.; Gong, K.; Chew, J. Molecular Interactions between a Lipid and an Antineoplastic Drug Paclitaxel (Taxol) within the Lipid Monolayer at the Air/Water Interface. *Langmuir* **2002**, *18* (10), 4061−4070.
(18) Liu, Y.; Huang, L.; Liu, F. Paclitaxel Nanocrystals for Overcoming Multidrug Resistance in Cancer. *Mol. Pharmaceutics* **2010**, *7* (3), 863−869.
(19) Wang, D.; Tang, J.; Wang, Y.; Ramishetti, S.; Fu, Q.; Racette, K.; Liu, F. Multifunctional Nanoparticles Based on a Single-Molecule Modification for the Treatment of Drug-Resistant Cancer. *Mol. Pharmaceutics* **2013**, *10* (4), 1465−9.
(20) Ma, Y.; Liu, D.; Wang, D.; Wang, Y.; Fu, Q.; Fallon, J. K.; Yang, X.; He, Z.; Liu, F. Combinational Delivery of Hydrophobic and Hydrophilic Anticancer Drugs in Single Nanoemulsions To Treat MDR in Cancer. *Mol. Pharmaceutics* **2014**, *11* (8), 2623−30.
(21) Yang, X.; Wang, D.; Ma, Y.; Zhao, Q.; Fallon, J. K.; Liu, D.; Xu, X. E.; Wang, Y.; He, Z.; Liu, F. Theranostic Nanoemulsions: Codelivery of Hydrophobic Drug and Hydrophilic Imaging Probe for Cancer Therapy and Imaging. *Nanomedicine* **2014**, 1−13.
(22) Giacomelli, C.; Borsali, R. Morphology of Poly(ethylene oxide)-block-Polycaprolatone Block Copolymer Micelles Controlled via the Preparation Method. *Macromol. Symp.* **2006**, *245−246* (1), 147−153.
(23) Yang, Y.; Hua, C.; Dong, C.-M. Synthesis, Self-Assembly, and In Vitro Doxorubicin Release Behavior of Dendron-like/Linear/Dendron-like Poly(ε-caprolactone)-b-Poly(ethylene glycol)-b-Poly(ε-caprolactone) Triblock Copolymers. *Biomacromolecules* **2009**, *10* (8), 2310−2318.
(24) Jain, S.; Bates, F. S. On the Origins of Morphological Complexity in Block Copolymer Surfactants. *Science* **2003**, *300* (5618), 460−464.
(25) Qian, J.; Zhang, M.; Manners, I.; Winnik, M. A. Nanofiber Micelles from the Self-Assembly of Block Copolymers. *Trends Biotechnol.* **2010**, *28* (2), 84−92.
(26) Sila, M.; Au, S.; Weiner, N. Effects of Triton X-100 Concentration and Incubation Temperature on Carboxyfluorescein Release from Multilamellar Liposomes. *Biochim. Biophys. Acta, Biomembr.* **1986**, *859* (2), 165−170.
(27) Chen, G.; Jiang, Z.; Yoshimoto, M.; Wei, Y. Electric Impedance Method for Evaluation of the Release Property of Calcein-Encapsulated Liposomes. *Colloids Surf., B* **2009**, *74* (1), 32−6.
(28) Letchford, K.; Burt, H. M. Copolymer Micelles and Nanospheres with Different In Vitro Stability Demonstrate Similar Paclitaxel Pharmacokinetics. *Mol. Pharmacol.* **2011**, *9* (2), 248−260.